INTERNATIONAL JOURNAL FOR NUMERICAL METHODS IN FLUIDS, VOL. 17, 349–364 (1993)

A FINITE ELEMENT SOLUTION OF THE TIME-DEPENDENT INCOMPRESSIBLE NAVIER–STOKES EQUATIONS USING A MODIFIED VELOCITY CORRECTION METHOD

GUANG REN* AND TORBJØRN UTNES

Department of Structural Engineering, N-7034 Trondheim, Norway

SUMMARY

A finite element solution of the two-dimensional incompressible Navier–Stokes equations has been developed. The present method is a modified velocity correction approach. First an intermediate velocity is calculated, and then this is corrected by the pressure gradient which is the solution of a Poisson equation derived from the continuity equation. The novelty, in this paper, is that a second-order Runge–Kutta method for time integration has been used. Discretization in space is carried out by the Galerkin weighted residual method. The solution is in terms of primitive variables, which are approximated by polynomial basis functions defined on three-noded, isoparametric triangular elements. To demonstrate the present method, two examples are provided. Results from the first example, the driven cavity flow problem, are compared with previous works. Results from the second example, uniform flow past a cylinder, are compared with experimental data.

KEY WORDS Finite elements Velocity correction method Flow past a cylinder Navier–Stokes equations

INTRODUCTION

Finite element methods are now widely used for fluid flow problems, and solution algorithms for the Navier–Stokes equations are described in numerous papers (see e.g. References 1–6). A number of different algorithms have been developed and impressive results were obtained from many of them.

The present paper is concerned with the solution of the incompressible Navier–Stokes equations for steady as well as time-dependent problems. We use a time-split, velocity correction formulation similar to the one described by Kovacs and Kawahara.[4] Variations of this method are used by several of the authors cited above. These formulations use a derived pressure equation to satisfy the continuity condition. This idea was first introduced by Chorin[7] in a finite difference context. Recently, many other authors have paid much attention to Chorin's idea and several variations of his method have been reported.[8–13]

The treatment of the advection terms in the momentum equations is another important issue to be addressed. A popular method is to use an explicit forward Euler time integration and include

* On leave from Dalian Maritime University, P. R. China

0271–2091/93/170349–16$13.00

Received July 1992
Revised February 1993

streamline diffusion (or balance tensor diffusion) in order to improve the stability.[1,4] A generalization of this method is the so called Taylor–Galerkin method, which can also be formulated as a two-step predictor–corrector method.[5] In this paper we use a second-order Runge–Kutta method for time integration instead of the formulations mentioned above.

The present method is tested on two different problems, namely the driven cavity problem and flow past a circular cylinder. The results from both of these tests are in good agreement with previous calculations or experimental data.

BASIC EQUATIONS

The basic equations are the two-dimensional incompressible Navier–Stokes equations and the continuity equation

$$\frac{\partial \mathbf{u}}{\partial t}+(\mathbf{u}\cdot\nabla)\mathbf{u}=-\frac{1}{\rho}\nabla p+\nu\nabla^2\mathbf{u}+\mathbf{g}, \tag{1}$$

$$\nabla\cdot\mathbf{u}=0$$

where $\mathbf{u}=(u, v)(\mathrm{m\,s^{-1}})$ is the velocity, p is the pressure ($\mathrm{N\,m^{-2}}$), t is time (s), ν is the kinematic viscosity ($\mathrm{m^2\,s^{-1}}$), and $\mathbf{g}$ is the gravitational acceleration ($\mathrm{m\,s^{-2}}$). Boundary conditions are

$$\mathbf{u}=\hat{\mathbf{u}}(\mathbf{x}, t) \quad \text{on} \quad \Gamma, \text{ with } \int_\Gamma \mathbf{n}\cdot\hat{\mathbf{u}}\,d\Gamma=0, \tag{2}$$

where $\hat{\mathbf{u}}$ is a known function on the boundary Γ of the domain Ω and $\mathbf{n}$ is the outward-pointing normal vector on Γ. Initial conditions are

$$\mathbf{u}=\mathbf{u}(x, t_0)=\mathbf{u}_0(x) \quad \text{in} \quad \Omega\cup\Gamma, \quad \text{with} \quad \nabla\cdot\mathbf{u}_0=0 \quad \text{in} \quad \Omega\cup\Gamma \tag{3}$$

where $\mathbf{u}_0$ is a prescribed function.

THE ALGORITHM

The algorithm is a modified velocity correction method described by Kovacs and Kawahara.[4] The difference between the present method and the original one is the scheme used for time integration. A second-order Runge–Kutta method has been used in the present algorithm. Computational results have shown that the numerical stability of the present method is good and very little additional computing time is required compared to an explicit Euler scheme. The algorithm is given as follows:

Step 1

Calculation of Runge–Kutta coefficients for an intermediate velocity $\tilde{u}$ omitting the pressure ($\nabla p^n/\rho$) and the gravitational ($\mathbf{g}$) terms.

$$\mathbf{K}_1=-\Delta t(-\nu\nabla^2\mathbf{u}^n+(\mathbf{u}^n\cdot\nabla)\,\mathbf{u}^n), \tag{4}$$

$$\mathbf{u}_k=\mathbf{u}^n+\mathbf{K}_1, \tag{5}$$

$$\mathbf{K}_2=-\Delta t(-\nu\nabla^2\mathbf{u}_k+(\mathbf{u}_k\cdot\nabla)\mathbf{u}_k). \tag{6}$$

Step 2

Calculation of an intermediate velocity field

$$\tilde{\mathbf{u}} = \mathbf{u}^n + \frac{\mathbf{K}_2 + \mathbf{K}_1}{2}. \tag{7}$$

Solution of the pressure Poisson equation to satisfy the incompressible continuity equation

$$\nabla^2 p^n = \left(\frac{\rho}{\Delta t}\right)(\nabla \cdot \tilde{\mathbf{u}}). \tag{8}$$

Step 4

Correction of the intermediate velocity field

$$\mathbf{u}^{n+1} = \tilde{\mathbf{u}} - \left(\frac{\Delta t}{\rho}\right)(\nabla p^n - \rho \mathbf{g}). \tag{9}$$

The superscript n indicates the nth time step, and Δt is the time increment.

THE FINITE ELEMENT METHOD

The finite element discretization of equations (4)–(9) is performed using the Galerkin weighted residual method through the following expansions in the piece-wise polynomial basis functions associated with the finite element method.

$$u(\mathbf{x}, t) = \sum_{i=1}^{N} u_i(t)\phi_i(\mathbf{x}), \tag{10}$$

$$p(\mathbf{x}, t) = \sum_{i=1}^{N} p_i(t)\phi_i(\mathbf{x}), \tag{11}$$

where N is the number of nodes for velocity and pressure in the discretized domain. The weak form of equations (4)–(9) permits $\phi_i(\mathbf{x})$ to be discontinuous in the first derivatives and introduces natural boundary conditions. Thus $\phi_i(\mathbf{x})$ are chosen to be C^0 piece-wise linear basis functions defined on isoparametric triangular elements. Inserting (10) and (11) into (4)–(9) leads to a discretized system of equations, which can be written in matrix from for the whole domain.

Step 1

$$\mathbf{M}\mathbf{K}_1 = -\Delta t \mathbf{S}^n \mathbf{u}^n - \Delta t \mathbf{A}^n \mathbf{u}^n + \Delta t \Gamma_u^n, \tag{12}$$

$$\mathbf{M}\mathbf{u}_k = \mathbf{M}\mathbf{u}^n + \mathbf{M}\mathbf{K}_1, \tag{13}$$

$$\mathbf{M}\mathbf{K}_2 = -\Delta t \mathbf{S}^n \mathbf{u}_k - \Delta t \mathbf{A}^n \mathbf{u}_k + \Delta t \Gamma_u^n. \tag{14}$$

Step 2

$$\mathbf{M}\tilde{\mathbf{u}} = \mathbf{M}\mathbf{u}^n + \left(\frac{\mathbf{M}\mathbf{K}_2 + \mathbf{M}\mathbf{K}_1}{2}\right). \tag{15}$$

Step 3

$$\mathbf{S}_p^n \mathbf{p}^n = -\left(\frac{\rho}{\Delta t}\right)(\mathbf{D}_x \tilde{\mathbf{u}} + \mathbf{D}_y \tilde{\mathbf{v}}) + \Gamma_p^n. \tag{16}$$

Step 4

$$\mathbf{M}\mathbf{u}^{n+1} = \mathbf{M}\tilde{\mathbf{u}} - \left(\frac{\Delta t}{\rho}\right)(\mathbf{D}p^n - \rho\mathbf{M}\mathbf{g}). \tag{17}$$

Here $\mathbf{u}^{n+1}$ and $\mathbf{u}^n$ are now global vectors containing all nodal values of (u, v) at the $(n+1)$th and nth time steps, respectively, $\tilde{\mathbf{u}}$ is the global vector for the intermediate velocity field, p^n is the global pressure vector containing all nodal values of p at the nth time step (p is defined on the same nodes as u), Γ_u^n and Γ_p^n are the vectors of natural boundary conditions for velocity and pressure respectively, $\mathbf{M}$ is the mass matrix, $\mathbf{S}^n$ is the diffusion or Laplacian matrix, and $\mathbf{A}^n = \mathbf{A}(\mathbf{u}^n)$ is the advection matrix.

The element matrices associated with equations (12)–(17) are evaluated on each element as:

$$\mathbf{M}^e = \int_A \boldsymbol{\Phi}\boldsymbol{\Phi}^{\mathrm{T}}\,\mathrm{d}A, \qquad \mathbf{S}_p^{en} = \int_A \left(\left(\frac{\partial \boldsymbol{\Phi}}{\partial x}, \frac{\partial \boldsymbol{\Phi}}{\partial y}\right) \begin{bmatrix} \dfrac{\partial \boldsymbol{\Phi}^{\mathrm{T}}}{\partial x} \\ \dfrac{\partial \boldsymbol{\Phi}^{\mathrm{T}}}{\partial y} \end{bmatrix} \right) \mathrm{d}A, \quad \mathbf{S}^{en} = \int_A \left(\left(\frac{\partial \boldsymbol{\Phi}}{\partial x}, \frac{\partial \boldsymbol{\Phi}}{\partial y}\right) \nu \begin{bmatrix} \dfrac{\partial \boldsymbol{\Phi}^{\mathrm{T}}}{\partial x} \\ \dfrac{\partial \boldsymbol{\Phi}^{\mathrm{T}}}{\partial y} \end{bmatrix} \right) \mathrm{d}A$$

$$\mathbf{D}_x^e = \int_A \boldsymbol{\Phi}\left(\frac{\partial \boldsymbol{\Phi}^{\mathrm{T}}}{\partial x}\right)\mathrm{d}A, \; \mathbf{D}_y^e = \int_A \boldsymbol{\Phi}\left(\frac{\partial \boldsymbol{\Phi}^{\mathrm{T}}}{\partial y}\right)\mathrm{d}A, \qquad \mathbf{D}^e = \begin{bmatrix} \mathbf{D}_x^e & 0 \\ 0 & \mathbf{D}_y^e \end{bmatrix},$$

$$\mathbf{A}^{en} = \int_A \boldsymbol{\Phi}\left[u^{n\mathrm{T}}\boldsymbol{\Phi}\left(\frac{\partial \boldsymbol{\Phi}^{\mathrm{T}}}{\partial x}\right) + v^{n\mathrm{T}}\boldsymbol{\Phi}\left(\frac{\partial \boldsymbol{\Phi}^{\mathrm{T}}}{\partial x}\right)\right]\mathrm{d}A,$$

where $\boldsymbol{\Phi}^{\mathrm{T}} = (\phi_1, \phi_2, \phi_3)$ is the vector of basis functions for an element.

STABILITY

The numerical stability of this scheme is limited by the advection–diffusion equation in the velocity prediction step. A simplified analysis for the one-dimensional case may be performed analogous to Baker and Kim,[14] and yields the condition

$$C < \frac{Pe}{(2+Pe)}, \tag{18}$$

where $C = U \cdot \mathrm{d}t/\mathrm{d}x$ is the Courant number, and $Pe = U \cdot \mathrm{d}x/\nu$ is the Peclet number. This result is valid if the mass matrix is lumped, which is the case in the present computations.

NUMERICAL EXAMPLES

Driven cavity flow

The classical driven cavity flow is chosen as the first example because it seems to be a standard test and there are documented data available for comparison. Reynolds numbers $Re = u_0 L/\nu = 1000$ and $Re = 3200$ are chosen. For $Re = 1000$, a (32×32) mesh is generated as illustrated in Figure 1, with 1089 nodal points and 2048 elements. For $Re = 3200$, a (40×40) mesh is generated, and the total number of nodal points is 1681 with 3200 elements. The boundary conditions are the domain being a square area (1×1 m) with three walls fixed (zero velocity), and the upper wall sliding with constant velocity $u_0 = 1\ \mathrm{m\,s^{-1}}$. At the two upper corners $u = 0$, and at

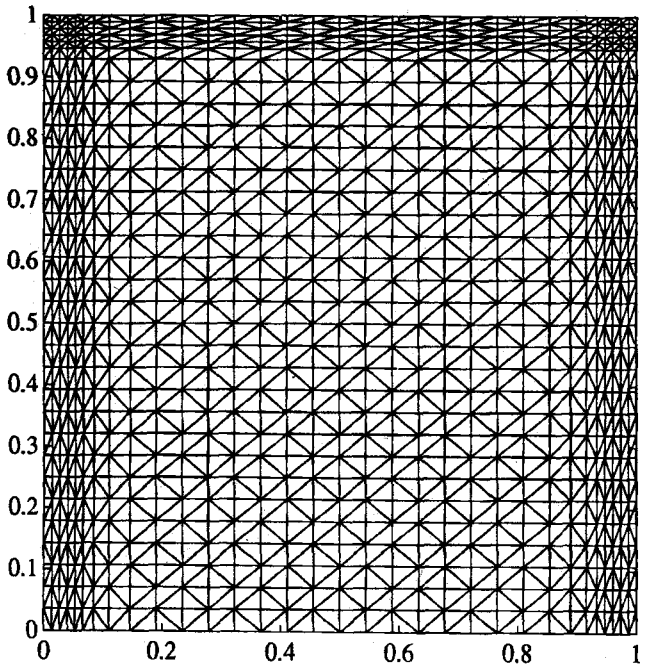

Figure 1. Mesh for cavity flow, $Re = 1000$

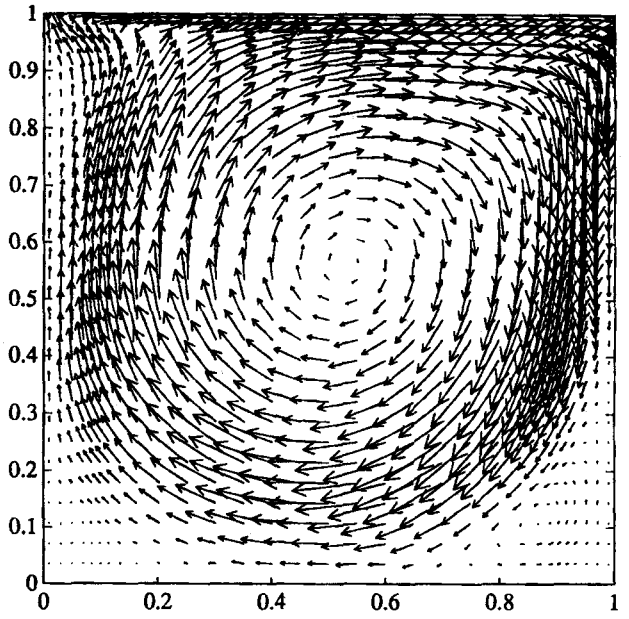

Figure 2. Velocity field of cavity flow, $Re = 1000$

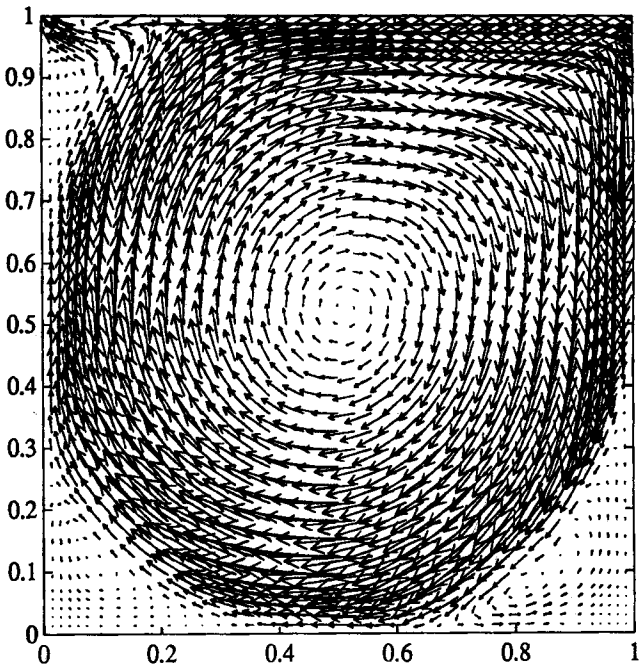

Figure 3. Velocity field of cavity flow, $Re = 3200$

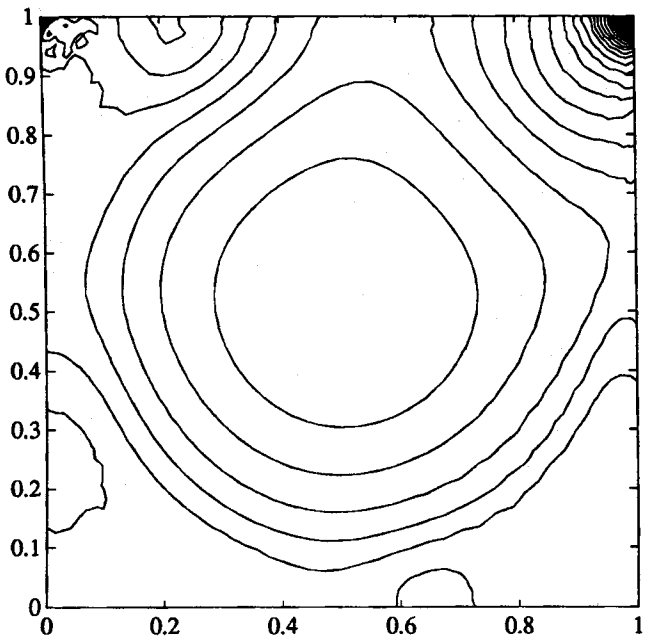

Figure 4. Pressure field of cavity flow, $Re = 3200$

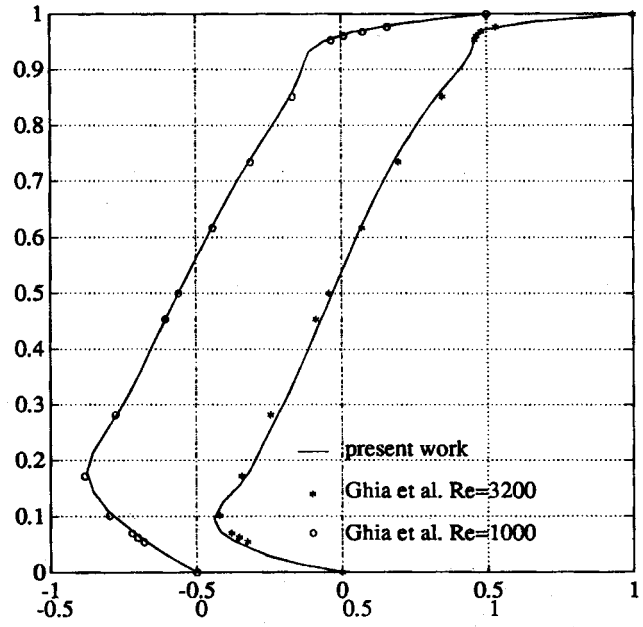

Figure 5. x-velocity distribution through geometric center of cavity, $Re = 1000$ and $Re = 3200$

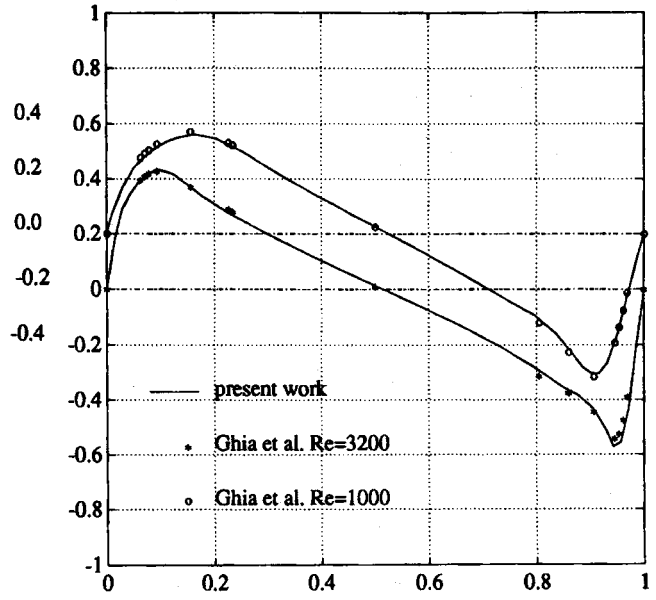

Figure 6. y-velocity distribution through geometric center of cavity, $Re = 1000$ and $Re = 3200$

the first node in from the corners $u=1/2$, as suggested by Sani *et al.*[15] At the middle point of the lower side of the cavity, the pressure is set to $p=0$. The time step is $\Delta t=0{\cdot}01$ s.

The computed velocity fields for $Re=1000$ and $Re=3200$ are illustrated in Figures 2 and 3. The pressure field for $Re=3200$ is shown in Figure 4. The results compare well with other calculations, for example Ghia *et al.*,[16] as shown in Figures 5 and 6. It should be noted that the present mesh is relatively coarse compared to the ones used by Ghia *et al.*[16] and Gresho *et al.*[3]

Flow past a circular cylinder

The modelling of viscous flow around a cylinder is of fundamental interest for several kinds of problems. Actual applications are, for example, the computation of flow around moving or fixed offshore constructions, underwater robotic vehicles, etc.[17,18]

The mesh for the present calculation is shown in Figure 7 and consists of 4363 nodes and 8404 elements. The diameter of the circular cylinder is chosen to be 0·005 m, the viscosity is 10^{-6} (water

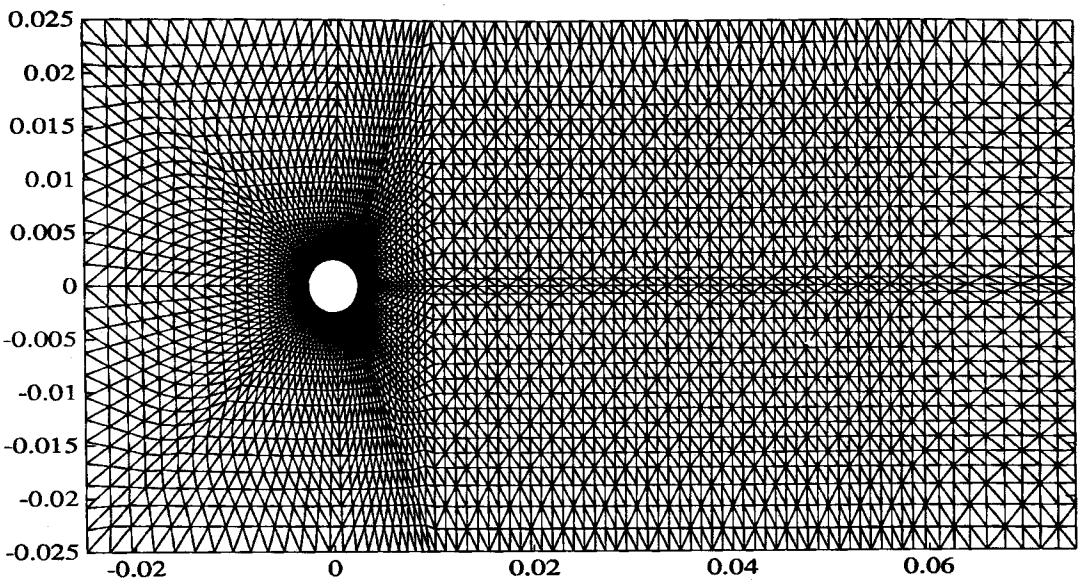

Figure 7. Mesh for flow around a cylinder. $Re=175$, 4363 nodes and 8404 elements

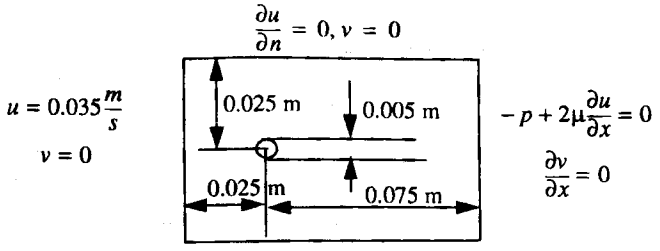

Figure 8. Boundary conditions for flow past a cylinder and parameters

at 20 °C), and the computational domain is $0{\cdot}05 \times 0{\cdot}1$ m. The Reynolds number based on the diameter of the cylinder is $Re = 175$. The boundary conditions and geometric parameters are illustrated in Figure 8. On the surface of the cylinder a no-slip boundary condition is imposed. The initial conditions are as follows. The flow is originally uniform with $u = 0{\cdot}035$ m s^{-1}. After the first time step, the boundary conditions given in Figure 8 are imposed. The time step is chosen to be $\Delta t = 0{\cdot}001$ s.

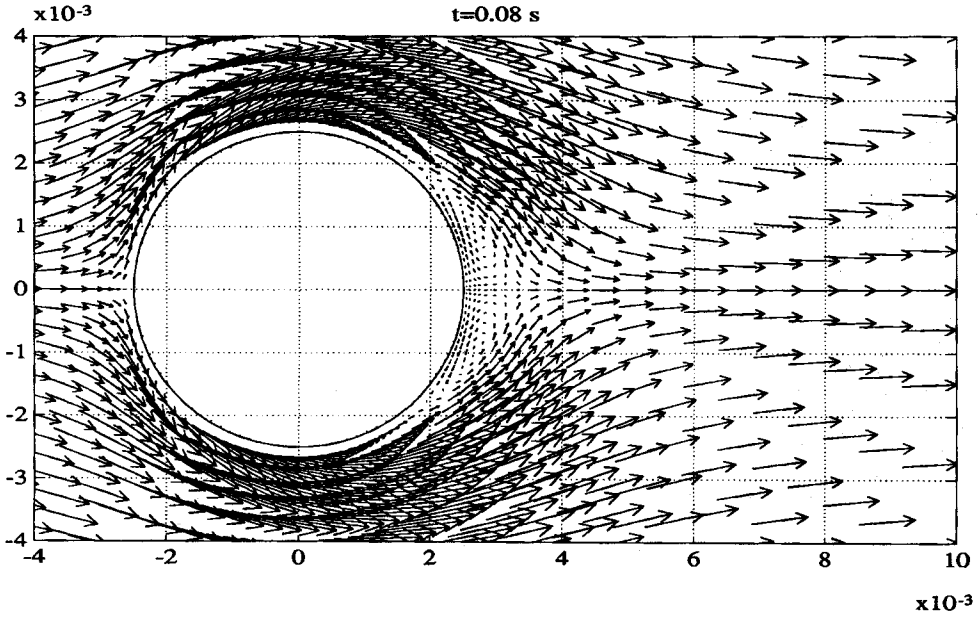

Figure 9. Velocity field of flow past a cylinder at time $t = 0{\cdot}08$ s, $Re = 175$

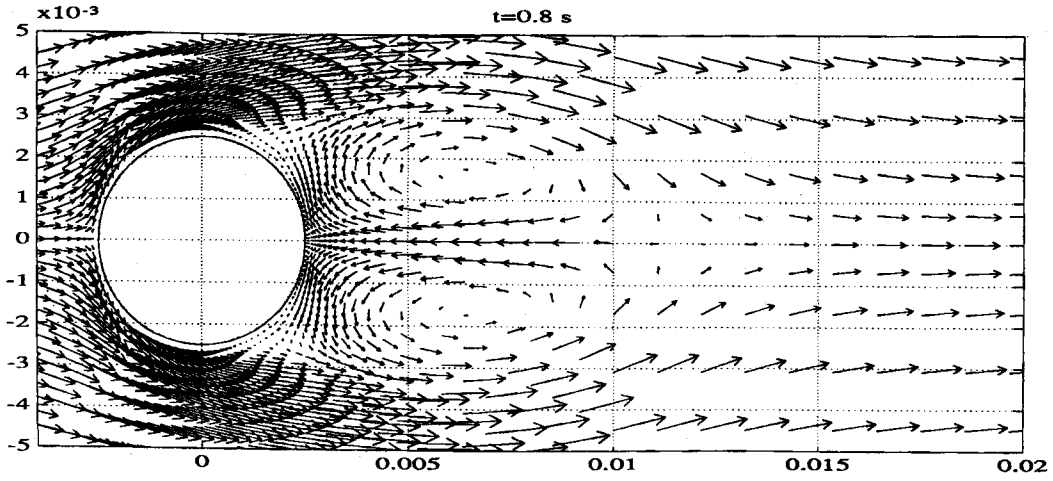

Figure 10. Velocity field of flow past a cylinder at time $t = 0{\cdot}8$ s, $Re = 175$

The time development of the flow is illustrated in Figures 9–16. The velocity field at time $t=0{\cdot}08$ s is shown in Figure 9, where two symmetric eddies can be seen. These phenomena are in good agreement with experimental data.[19] The velocity field at time $t=0{\cdot}8$ s is shown in Figure 10 and illustrates that the two eddies are enlarged along the x-direction. After $t=4{\cdot}0$ s the symmetry of the flow has disappeared and the vortex street starts to develop, as indicated in Figures 11 and 13. The vortex street is fully developed at $t=6{\cdot}85$ s as shown in Figure 15. Figures 15 and 16 illustrate the same situation for the velocity field in different co-ordinate frames. Figure 15 is seen from a cylinder-fixed frame, while Figure 16 shows the velocity field in the flow-fixed frame. The

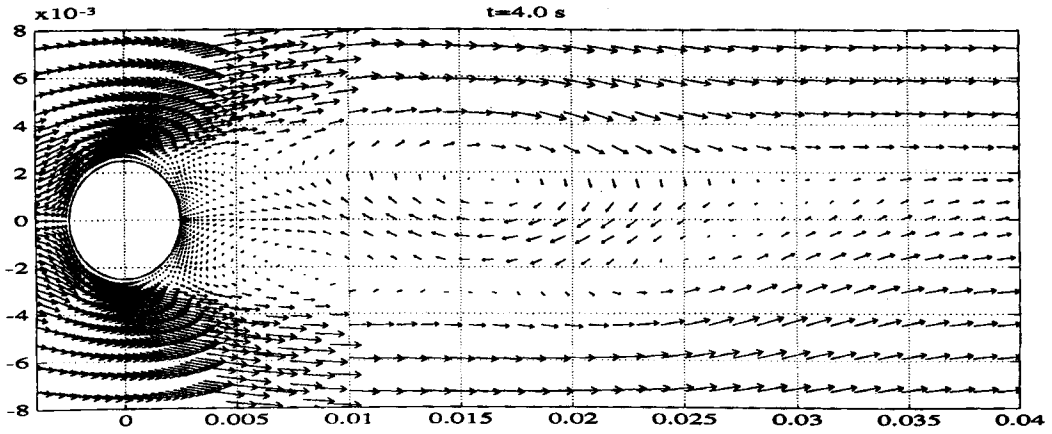

Figure 11. Velocity field at time $t=4{\cdot}0$ s, $Re=175$

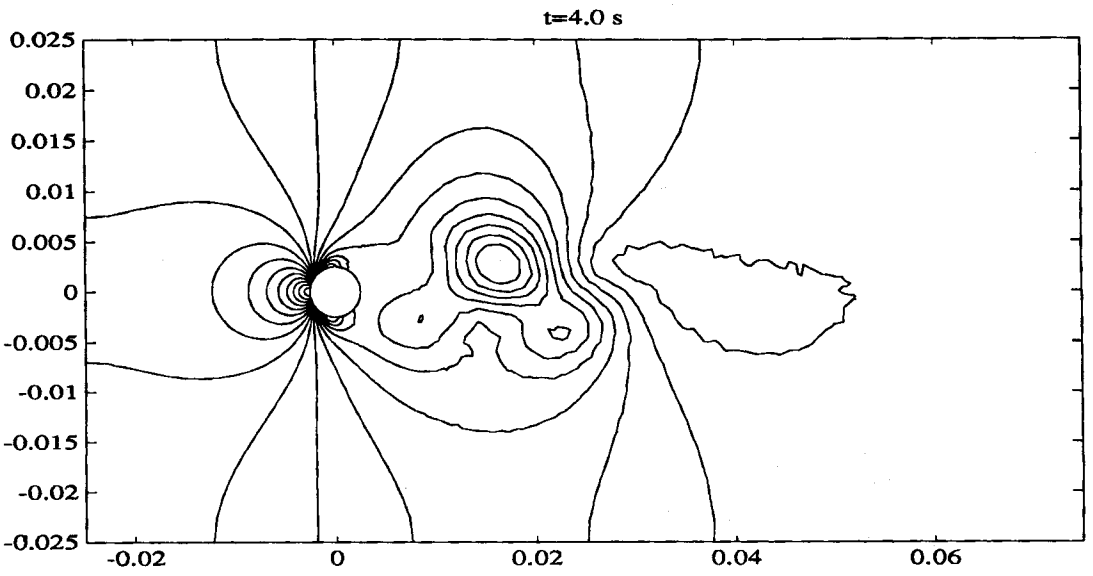

Figure 12. Pressure field at time $t=4{\cdot}0$ s, $Re=175$

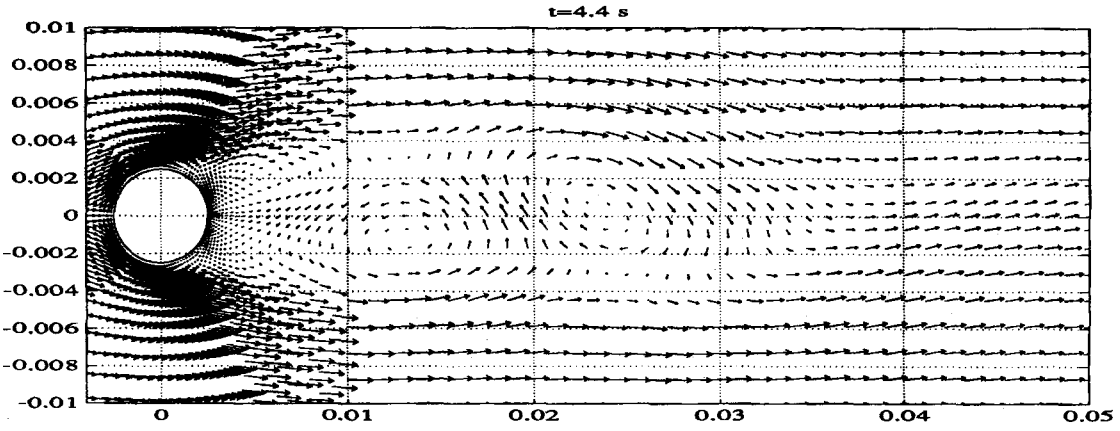

Figure 13. Velocity field at time $t=4{\cdot}4$ s, $Re=175$

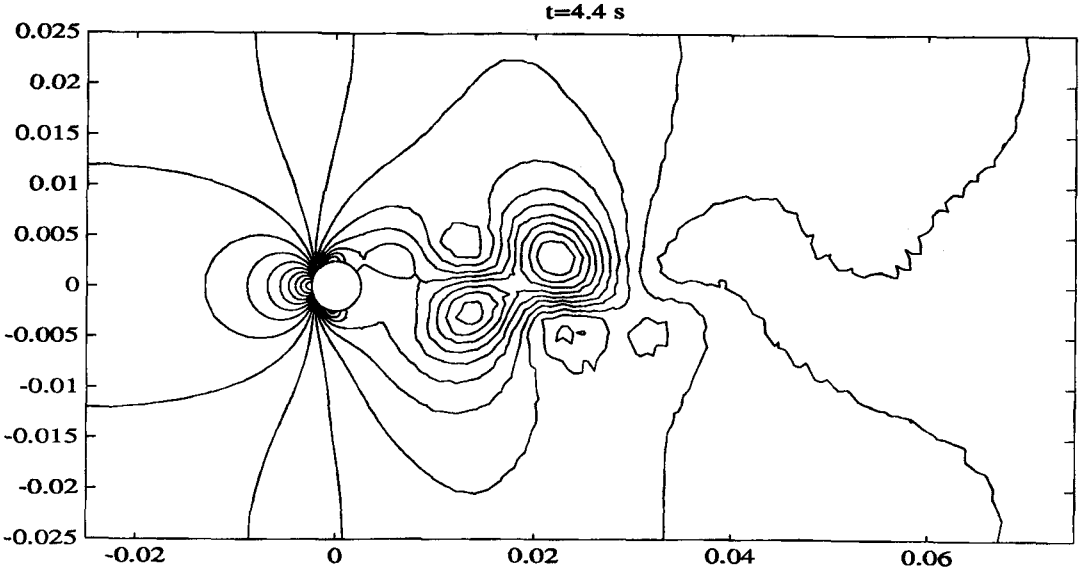

Figure 14. Pressure field at time $t=4{\cdot}4$ s, $Re=175$

latter illustrates the eddies in the wake more clearly than the former. This result is in good agreement with the experimental data presented by Prandtl and Tietjens.[19] A detailed numerical study of the vortex street behind a cylinder is given by Ren.[17]

Figure 17 illustrates a comparison between the present results and the experimental data for the mean pressure coefficient

$$C_p=\frac{(p-p_\infty)}{\frac{1}{2}\rho u_\infty^2}$$

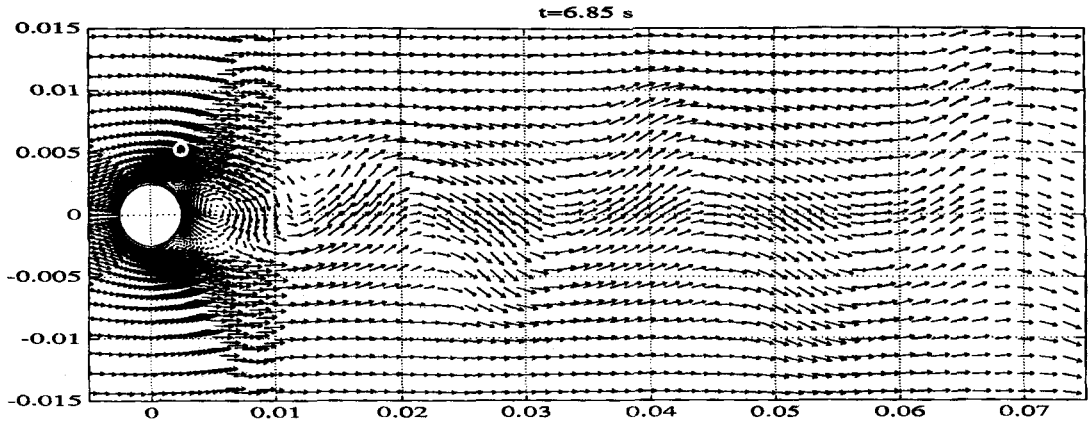

Figure 15. Velocity field at time $t=6{\cdot}85$ s, $Re=175$

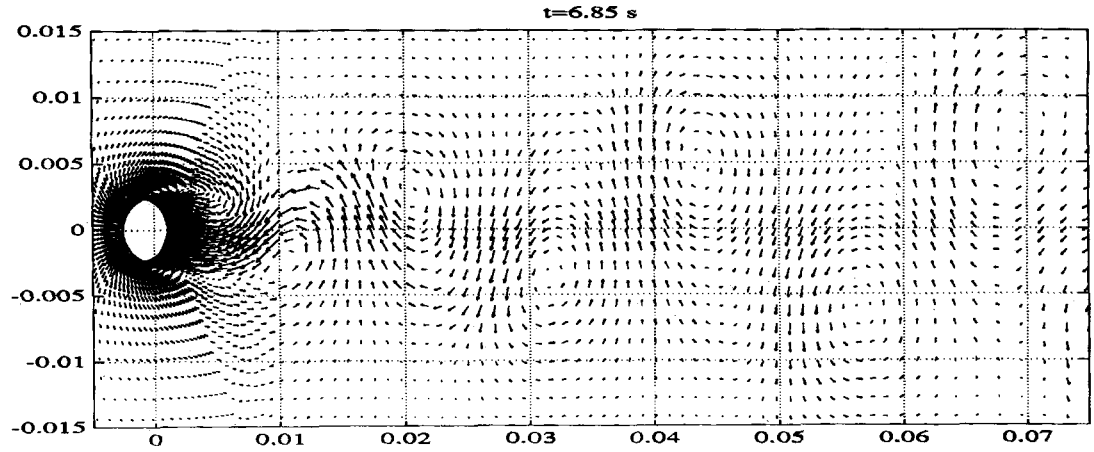

Figure 16. Velocity field seen from a flow-fixed co-ordinate frame at time $t=6{\cdot}85$ s, $Re=175$

on the cylinder surface. It is noted that there is a certain side-wall effect present due to the actual ratio of cylinder to tunnel width, d/h, where d is diameter of the cylinder, and h is the width of the tunnel. Our results agree well with the experimental data from Grove *et al.*[20]

DISCUSSION

(1) Corner singularities

For the cavity problem, the boundary conditions at the upper corners may produce singularities. Figure 18 illustrates the effect of applying two different conditions. One is to specify $u=1/2$ at the corners, and the other is to put $u=0$ at the corners and $u=1/2$ at the next point from the corners. The latter condition was suggested by Sani *et al.*[15] to avoid a spurious pressure mode and this condition has been used in our computations.

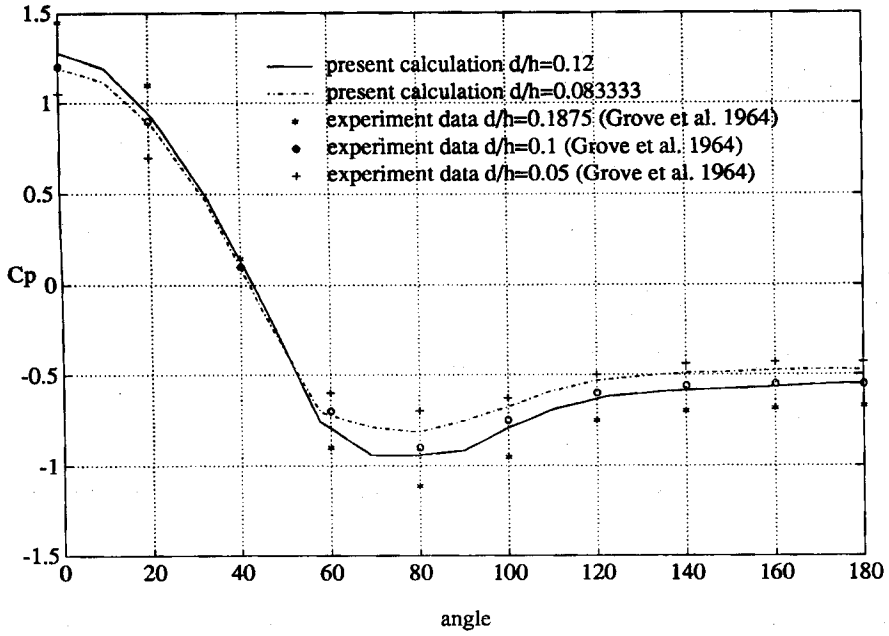

Figure 17. Comparison of pressure coefficients with experimental data, $Re = 175$

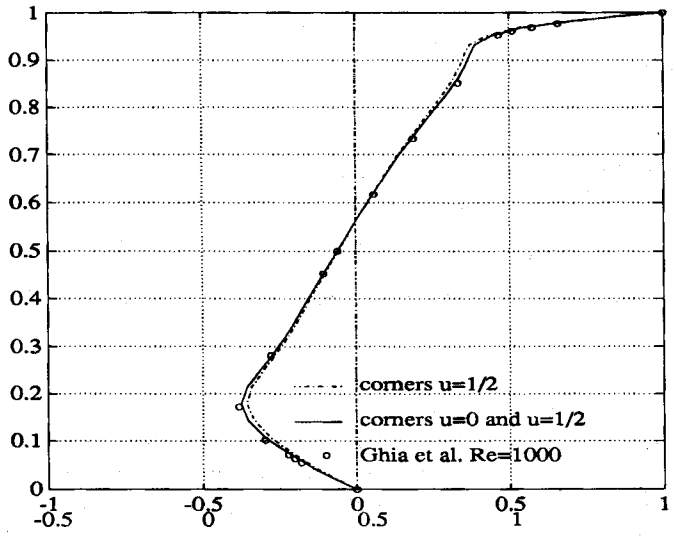

Figure 18. The effect of spurious pressure on the result of the cavity flow problem, $Re = 1000$

(2) The mesh around the cylinder

In the second example, flow past a cylinder, the grid near the cylinder should be very fine, otherwise the numerical transient process will be much delayed. Figures 19 and 20 illustrate results computed on a coarse mesh with 3120 elements and 1655 nodal points. Other conditions

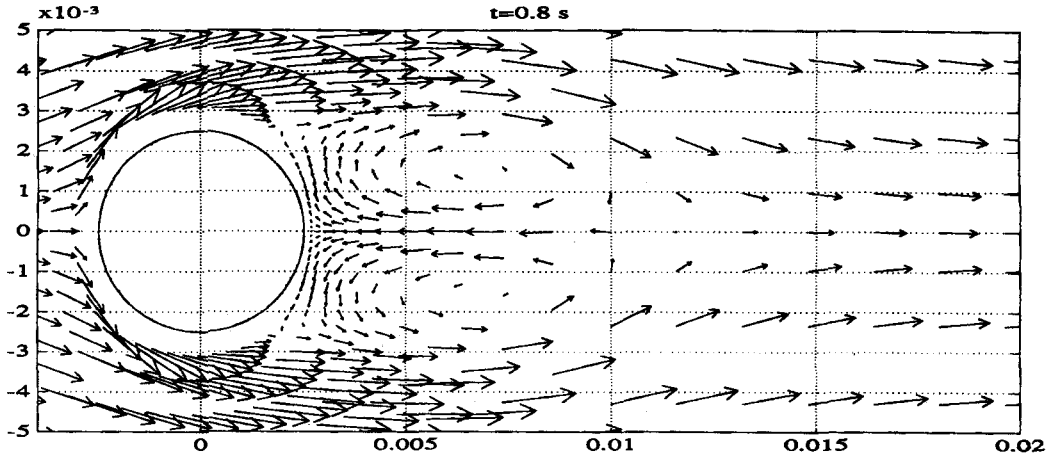

Figure 19. Velocity field computed on a coarse mesh, N-point = 1655, N-element = 3120, $t = 0{\cdot}8$ s, $Re = 175$

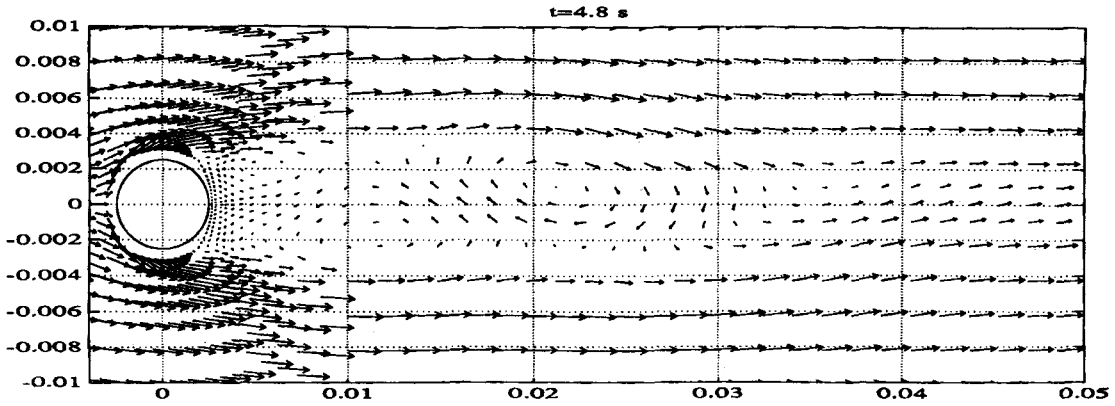

Figure 20. Velocity field computed on a coarse mesh, $t = 4{\cdot}8$ s, $Re = 175$

are the same as before. At time $t = 0{\cdot}8$ s there is not much difference between results computed from the coarse mesh or the fine mesh (compare Figure 19 with Figure 10). However, after time $t > 4$ s, the time delay of the vortex street development can be seen clearly (compare Figure 20 with Figure 13 and note that time is $t = 4{\cdot}8$ s in Figure 20 while $t = 4{\cdot}4$ in Figure 13). The main reason may be that the non-linear Navier–Stokes equations cannot be resolved on the coarse mesh without loss of accuracy.

(3) The outflow boundary condition

In the example of flow past a cylinder, two types of outflow boundary conditions for the pressure have been tested. One is to prescribe a constant pressure $p = 0$. The other is to use a traction-free condition, $-p + 2\mu(\partial u/\partial x) = 0$ (see Reference 21). The traction-free boundary condition may be better than the first one when the vortex street is fully developed. The pressure

field obtained from the latter condition is more regular than that obtained from using $p=0$. We implement the traction-free condition in the solution of the Poisson equation and the pressure on the outflow boundary is calculated from the known velocity as

$$p_i = 2\mu \frac{u_{i+1} - u_i}{\mathrm{d}x}, \tag{19}$$

where p_i is the pressure on the outflow boundary, u_i is the velocity on the outflow boundary, u_{i+1} is the first nodal point inside the outflow boundary in the x-direction, and dx is the distance from point of x_i to x_{i+1}.

(4) The code

The program is written in the C programming language and compiled and run on a SUN/Sparc Station. We have used two methods to solve the Poisson equation. One is the Gaussian elimination method, taking account of the symmetric band-structure of the stiffness matrix. The other is the so-called skyline solver. Our numerical tests show that the latter is several times faster than the former, depending on the number of total points and the bandwidth of the assembly system. We recommend the skyline solver method. To represent the results, MATLAB has been used.

CONCLUSIONS

A finite element solution of the Navier–Stokes equations has been presented. The method is a modified velocity correction scheme. A second-order Runge–Kutta method has been used for the time integration of the intermediate velocity integration in order to improve the numerical stability and time-integration accuracy compared to an explicit Euler scheme. Numerical examples have shown that the present results are in good agreement with the experimental data.

ACKNOWLEDGEMENTS

The authors wish to thank Professor Jens G. Balchen at the Division of Engineering Cybernetics, the Norwegian Institute of Technology, for valuable support and the referees for their valuable comments and suggestions.

REFERENCES

1. P. M. Gresho, S. T. Chan, R. L. Lee and C. D. Upson, 'A modified finite element method for solving the time-dependent incompressible Navier–Stokes equations. Part 1: theory', *Int. j. numer. methods fluids*, **4**, 557–598 (1984).
2. T. Utnes, 'Finite element modelling quasi-three-dimensional nearly horizontal flow', *Int. j. numer. methods fluids*, **12**, 559–576 (1991).
3. P. M. Gresho, S. T. Chan, R. L. Lee and C. D. Upson, 'A modified finite element method for solving the time-dependent incompressible Navier–Stokes equations. Part 2: applications', *Int. j. numer. methods fluids*, **4**, 619–640 (1984).
4. A. Kovacs and M. Kawahara, 'A finite element scheme based on the velocity correction method for the solution of the time-dependent incompressible Navier–Stokes equations', *Int. j. numer. methods fluids*, **13**, 403–423 (1991).
5. O. C. Zienkiewicz and R. L. Taylor, *The Finite Element Method*, Vol. 2, McGraw-Hill, London, 1991.
6. P. M. Gresho, 'Incompressible fluid dynamics: some fundamental formulation issues', *Ann. Rev. Fluid Mech.*, **23**, 413–453 (1991).
7. A. J. Chorin, 'Numerical solution of the Navier–Stokes equations', *Math. Comput.*, **22**, 745–762 (1968).
8. J. Kim and P. Moin, 'Application of a fractional-step method to incompressible Navier–Stokes equations', *J. Comput. Phys.*, **59**, 308–323 (1985).

9. P. M. Gresho, 'On the theory of semi-implicit projection methods for viscous incompressible flow and its implementation via a finite element method that also introduces a nearly consistent mass matrix. Part 1: theory', *Int. j. numer. methods fluids*, **11**, 587–620 (1990).
10. R. Natarajan, 'A numerical method for incompressible viscous flow simulation', *J. Comput. Phys.*, **100**, 384–395 (1992).
11. J. B. Bell and D. L. Marcus, 'A second-order projection method for variable-density flow', *J. Comput. Phys.*, **101**, 334–348 (1992)
12. J. Zhu and J. Sethian, 'Projection methods coupled to level set interface techniques', *J. Comput. Phys.*, **102**, 128–138 (1992).
13. J. K. Dukowicz, 'Approximate fractorization as a high order splitting for the implicit incompressible flow equations', *J. Comput. Phys.*, **102**, 336–347 (1992).
14. A. J. Baker and J. W. Kim, 'A Taylor weak-statement algorithm for hyperbolic conservation laws', *Int. j. numer. methods fluids*, **7**, 489–520 (1987).
15. R. L. Sani, P. M. Gresho, R. L. Lee, D. F. Griffiths and M. Engelman, 'The cause and cure (!) of the spurious pressures generated by certain FEM solutions of the incompressible Navier–Stokes equations: Part 2', *Int. j. numer. methods fluids*, **1**, 171–204 (1981).
16. U. Ghia, K. N. Ghia and C. T. Shin, 'High-Re solution for incompressible flow using the Navier–Stokes equations and a multigrid method', *J. Comput. Phys.*, **48**, 387–411 (1982).
17. G. Ren, 'Finite element modelling the hydrodynamic environment of AUV', *Ph.D. Thesis*, Norwegian Institute of Technology, Trondheim, Norway, 1992.
18. T. I. Fossen, Nonlinear Modelling and Control of Underwater Vehicles, *Ph.D. Thesis*, Norwegian Institute of Technology, Trondheim, Norway, 1991.
19. L. Prandtl and O. G. Tietjens, *Applied Hydro- and Aeromechanics*, Dover, New York, 1934.
20. A. S. Grove, F. H. Shair, E. E. Petersen and A. Acrivos, 'An experimental investigation of the separated flow past a circular cylinder', *J. Fluid Mech.*, **19**, 60–80 (1964).
21. P. M. Gresho, R. L. Lee and R. L. Sani, 'On the time-dependent solution of the incompressible Navier–Stokes equations in two and three dimensions', in C. Taylor and K. Morgan (eds), *Recent Advances In Numerical Methods in Fluids*, 1980, pp. 27–79.